ANNUAL REVIEWS

Annual Review of Biophysics

Structure of Phycobilisomes

Sen-Fang Sui

State Key Laboratory of Membrane Biology, Beijing Advanced Innovation Center for Structural Biology and Frontier Research Center for Biological Structure, School of Life Sciences, Tsinghua University, Beijing 100084, China; email: suisf@mail.tsinghua.edu.cn

Annu. Rev. Biophys. 2021. 50:53–72

The *Annual Review of Biophysics* is online at biophys.annualreviews.org

https://doi.org/10.1146/annurev-biophys-062920-063657

Keywords

phycobilisome, cryo-EM, red algae, linker protein, π–π interactions, energy transfer in photosynthesis

Abstract

Phycobilisomes (PBSs) are extremely large chromophore–protein complexes on the stromal side of the thylakoid membrane in cyanobacteria and red algae. The main function of PBSs is light harvesting, and they serve as antennas and transfer the absorbed energy to the reaction centers of two photosynthetic systems (photosystems I and II). PBSs are composed of phycobiliproteins and linker proteins. How phycobiliproteins and linkers are organized in PBSs and how light energy is efficiently harvested and transferred in PBSs are the fundamental questions in the study of photosynthesis. In this review, the structures of the red algae *Griffithsia pacifica* and *Porphyridium purpureum* are discussed in detail, along with the functions of linker proteins in phycobiliprotein assembly and in fine-tuning the energy state of chromophores.

Contents

1. INTRODUCTION TO PHYCOBILISOMES

Life on earth predominantly depends on photosynthesis for the conversion of solar energy to chemical energy. The photosynthetic machinery is composed of two principal parts: the light-harvesting antenna and the photochemical reaction centers (46). To obtain light energy efficiently, organisms living in different environments have developed a variety of light-harvesting systems. The membrane-intrinsic light-harvesting complexes (LHCs) mainly exist in green algae and high plants, whereas the membrane-extrinsic soluble phycobilisomes (PBSs) are responsible for the majority of light capture in cyanobacteria and red algae (2, 40). Although PBSs are the largest light-harvesting antennae (3 MDa–18 MDa) and contain hundreds to thousands of chromophores [e.g., the red algae *Griffithsia pacifica* (Gp) has 2,048 bilins (97), and *Porphyridium purpureum* (Pp) has 1,598 bilins (57)], loss of energy is minimal in the process of energy transfer. Many recent achievements have improved our understanding of the mechanism of this extremely highly efficient energy transfer complex over the years, including spectral analyses and structural studies of phycobiliproteins (PBPs), linker proteins, and entire PBSs. This review focuses on recent advances in high-resolution structures of the intact PBSs and their implications for identifying the energy transfer pathway.

1.1. Discovery and Isolation of Phycobilisomes for Structural Research

PBSs were first discovered as small granules on the stromal side of the thylakoid of the red alga *Porphyridium cruentum* by Gantt & Conti (33) and were named after the phycobilins found in PBSs (34). Intact PBSs were first isolated after thylakoid membranes were treated with

detergent followed by gradient ultracentrifugation (35), and their components were analyzed using biophysical, biochemical, and other methods (11, 40, 41, 59, 79).

Four main morphological types of PBSs were found: hemiellipsoidal (6), block-shaped (36), bundle-shaped (43), and hemidiscoidal. The hemidiscoidal PBSs can be further classified into PBSs with tricylindrical cores and six peripheral rods (93), those with two cores and six peripheral rods (95), and those with five cores and eight peripheral rods (25). Some uncommon rod-shaped PBSs have also been observed (45).

1.2. The Composition of Phycobilisomes

PBSs are composed of PBPs and linker proteins. PBPs are brilliantly colored, water-soluble proteins bearing different kinds of chromophores called bilins, which are open-chain tetrapyrroles and are covalently bound to cysteine residues via thioether bonds. On the basis of the bilin energy levels, PBPs are mainly categorized into three types: phycoerythrins (PEs) or phycoerythrocyanins at the core-distal ends of rods (which absorb high-energy light); phycocyanins (PCs) at the core-adjacent portions of rods (which absorb intermediate-energy light); and allophycocyanins (APCs), the major components of the core (which absorb low-energy light). Two different PBP subunits, α and β, initially form a heterodimer (αβ), conventionally called the (αβ) monomer, which subsequently assembles into the $(\alpha\beta)_3$ trimer. These trimers are the fundamental assembly unit of PBSs and stack face to face to form an $(\alpha\beta)_6$ hexamer with a linker protein in its central cavity. APCs in the core have a few variants, such as $\alpha^{L_{CM}}$ (the α domain in L_{CM}; L_{CM} is coded by *apcE*), the α^{APC}-like variant (denoted ApcD, coded by *apcD*), and the β^{APC}-like variant (denoted ApcF, coded by *apcF*).

Linkers can be classified into three groups based on their locations: L_{CM} and L_C in the core (L_{CM} also occurs between the core and thylakoid membranes), L_R in rods, and L_{RC} between the core and the rods. Although they are present in much lower numbers than PBPs, linkers govern the assembly of PBPs into PBSs and modulate the energy transfer process. Chromophored rod linkers (γ subunits) are also found in red algae, the marine cyanobacteria *Synechococcus*, and low-light-adapted *Prochlorococcus* (42). Recently, all linker protein structures of the red algae Gp and Pp were resolved from high-resolution cryo-electron microscopy (EM) structures of the entire PBSs (57, 97).

2. TOWARD AN ATOMIC-RESOLUTION STRUCTURE OF THE COMPLETE PHYCOBILISOME

2.1. Phycobilisome Structures by X-Ray Crystallography

To date, more than 30 structures of PBPs (including four types, PE, PC, APC, and phycoerythrocyanin) from different species have been resolved using X-ray crystallography (**Table 1**). Although PBPs have different absorption spectra due to different bilin energy levels, the $(\alpha\beta)_3$ trimers containing them have similar ring-like structures and assemble into PBSs through a common hierarchical organization.

The crystal structures of two terminal emitters demonstrated the relationship between structure and function. The ApcD subunit has more coplanar phycocyanobilin (PCB) bilin than does the ApcA subunit, which can be attributed to the amino acid sidechains surrounding the bilins (68). The PCB bilin in $\alpha^{L_{CM}}$ displays a conformational change from the *ZZZasa* of ApcA's PCB to a more coplanar conformer *ZZZssa* (86). Higher coplanarity of PCBs results in a lower energy level; thus, these two subunits can function as the terminal emitters to funnel the absorbed energy from PBSs to photosystem I (PSI) or photosystem II (PSII).

Table 1 Crystal structures of PBP rigid domains

Species	PBP type	PDB code	Asymmetric unit	Resolution (Å)	Reference
Mastigocladus laminosus	C-PC	NA	(αβ)	2.1	75, 76
Synechococcus sp. PCC7002	PC	NA	$(\alpha\beta)_3$	2.5	77
Mastigocladus laminosus	PEC	NA	(αβ)	2.7	26
Fremyella diplosiphon	C-PC	1CPC	(αβ)	1.66	27
Porphyridium sordidum	B-PE	NA	2 × (αβ)	2.2	29
Spirulina platensis	APC	1ALL	(αβ)	2.3	9
Polysiphonia urceolata	R-PE	1LIA	$(\alpha\beta)_3$	2.8	17
Porphyra yezoensis	APC	1KN1	(αβ)	2.2	54
Mastigocladus laminosus	APC.$L_{C\,7.8}$	1B33	2 × $(\alpha\beta)_3$	2.2	70
Griffithsia monilis	PE	1B8D	2 × (αβ)	1.9	71
Rhodomonas CS24	PE 545	1QGW	$(\alpha_1\alpha_2\beta\beta)$	1.63	92
Cyanidium caldarium	C-PC	1PHN	2 × (αβ)	1.65	84
Gracilaria chilensis	R-PE	1EYX	2 × (αβ)	2.2	18
Polysiphonia urceolata	PC	1F99	$(\alpha\beta)_3$	2.4	49
Spirulina platensis	C-PC	1GH0	2 × $(\alpha\beta)_6$	2.2	89
	C-PC	1HA7	2 × $(\alpha\beta)_6$	2.2	67
Thermosynechococcus vulcanus	C-PC/PC 612	1I7Y/1KTP/1ON7	(αβ)	2.5/1.6/2.7	3–5
Thermosynechococcus elongates	C-PC	1JBO	(αβ)	1.45	66
Rhodomonas CS24	PE 545	1XF6/1XG0	$(\alpha_1\alpha_2\beta\beta)$	1.1/0.97	24
Mastigocladus laminosus	PECα	2C7J/2C7K/2C7L	(αβ)	2.85	78
Gracilaria chilensis	PC-PC	2BV8	$(\alpha\beta)_6$	2.0	19
Thermosynechococcus elongatus	APC	2V8A	$(\alpha\beta)_3$	3.5	65
Thermosynechococcus vulcanus	APC	3DBJ	$(\alpha\beta)_3$	2.9	62
Phormidium tenue	F-αPE	3MWN	α	2.6	83
Synechocystis sp. PCC 6803	N-L_R	3NPH	L_R[30]	1.9	37
Porphyridium cruentum	B-PE	3V57/3V58	$(\alpha\beta)_3$	1.85/1.70	15
Synechocystis sp. PCC 6803/ *Synechococcus elongatus* sp. PCC 7942/*Thermosynechococcus vulcanus*	PC/APC	4F0T/4H0M/ 4F0U/4GXE/ 4GY3	(αβ)/$(\alpha\beta)_3$	2.25/2.2/2.5 3.0/2.5	61
Synechocystis sp. PCC 6803	AP-B	4PO5	$[(ApcD/ApcB)]_3$	1.75	68
Phormidium rubidum A09DM	APC	4RMP	$(\alpha\beta)_3$	2.51	80
Nostoc sp. PCC7120	$L_{CM}\Delta$	4XXI	$[(ApcE\Delta/ApcB)]_3$	2.2	86
Phormidium rubidum A09DM	C-PE	5AQD/5FVB	$(\alpha\beta)_6$	1.95/2.12	51
Gracilaria chilensis	APC	5TJF	$(\alpha\beta)_3$	2.3	21
Phormidium rubidum A09DM	C-PE	5NB4/5NB3	$(\alpha\beta)_6$	1.14/1.38	82
Phormidium rubidum A09DM	PC	6XWK	$(\alpha\beta)_3$	1.71	81

Abbreviations: APC, allophycocyanin; NA, not applicable; PBP, phycobiliprotein; PC, phycocyanin; PDB, Protein Data Bank; PE, phycoerythrin; PEC, phycoerythrocyanin.

The structures of full-length linkers have not been solved to date using X-ray crystallography, possibly because of the nature of isolated full-length linkers, which contain very high amounts of flexible loops that restrict their crystallization. Although linkers can be cocrystallized with PBP trimers or hexamers, the intrinsic asymmetry of linkers results in their loss of information in the

central hole of C3 symmetric PBP trimers (71). Thus, only two rigid domains of linkers have been resolved using X-ray crystallography to date.

2.2. Phycobilisome Structures by Electron Microscopy

Given their huge size, PBSs are great samples for EM studies. However, although EM research on PBSs began in the 1960s, most breakthroughs were only achieved in the past few years due to the development of the cryo-EM instrumentation, computational methodology, and technology of sample preparation (**Table 2**).

Two main challenges were encountered when cryo-EM was applied to studying the structure of PBSs. One problem is the sample preparation: Isolated intact PBSs require a high concentration of phosphate (0.6–1.0 mol·L^{-1}) to maintain their integrity in aqueous solution, which leads to poor contrast of micrographs in cryo-EM. The other problem is the preferential orientation of the intact PBSs under cryo-EM imaging. This is similar to their natural orientation: Only one side of the PBS preferentially attaches to thylakoids. To overcome the first problem, samples on grids were frozen after being quickly mixed with the phosphate-free buffer to reduce the salt concentration and keep the sample integrity. To resolve the second problem, different views were observed by changing the electrical properties of copper mesh. After a series of improvements in sample preparation, the first near-atomic structure of the intact PBS from Gp (GpPBS) at 3.5 Å was obtained using single-particle cryo-EM in 2017 (97). Structures of all 17 types of linkers in this PBS were resolved, and the spatial arrangement of all 2,048 bilins was also determined. Subsequently, in 2020, the cryo-EM structure of the intact hemiellipsoidal PBS from Pp (PpPBS) was resolved at a markedly improved resolution—2.8 Å (57), which enabled the building of an accurate atomic model of the PpPBS with higher confidence.

3. OVERALL STRUCTURE OF PHYCOBILISOMES

The overall structures from the block-shaped GpPBS and the hemiellipsoildal PpPBS are very similar (**Figure 1*a***). Both of them contain a pyramid-shaped core with the top cylinder (formed by two APC trimers stacked back to back) sitting above two basal cylinders (each formed by one APC hexamer and one APC trimer), surrounded by 14 peripheral rods arranged in a staggered fashion. In addition to the core and rods, extra PE hexamers, as well as individual α- and β-subunits, fill in the empty spaces outside the core and rods, which may help to stabilize the PBS. The most striking feature of the PBS is the scaffold formed by the linker proteins (**Figure 1*b***).

3.1. Scaffold Formed by Linker Proteins

The structural models of PBSs from both Gp and Pp reveal that the PBP components of PBSs are organized together through the extended scaffold formed by the linker proteins. In the rods, the linker proteins interact with each other, leading to the formation of the rod skeletons (like spokes in a wheel going to the center), and the ring-shaped hexamers, having a hole in their center, are strung onto these skeletons. The linker proteins and APC trimers in the core come into close contact to form the compact core. The PBPs are assembled together by anchoring the rod skeletons onto the specific locations of the core (like the center of the wheel) (**Figure 1*c***).

This organization of the PBS is very similar to sugar-coated haws on a stick (Tang Hulu), a traditional Chinese snack that is popular among children (**Figure 1*d***). A string of sugar-coated haws are threaded together on a stick, and many sticks are then inserted into a straw block. Thus, the stick is analogous to the rod linker skeleton, the haw is analogous to the PBP hexamer, and the straw block is analogous to the core. Without the stick, the haws are dispersed. Without the straw block, many Tang Hulu cannot be fixed together in order.

Table 2 PBS structure studies using EM

Species	PBS type	PDB code	EMDB code	Methods	Resolution	Reference
Porphyridium cruentum	Red alga, hemiellipsoidal	NA	NA	NS	NA	32, 33, 35
Griffithsia pacifica	Red alga, block-shaped	NA	NA	NS	NA	36
Synechococcus sp., *Calothrix* sp.	Cyanobacterial, hemidiscoidal	NA	NA	NS	NA	11
Synechococcus 6301	Cyanobacterial, hemidiscoidal	NA	NA	NS	NA	95
Gloeobacter violaceus	Cyanobacterial, bundle-shaped	NA	NA	NS	NA	43
Synechocystis sp. PCC6803	Cyanobacterial, hemidiscoidal	NA	NA	NS	NA	28
Anabaena sp. PCC 7120	Cyanobacterial, hemidiscoidal	NA	NA	NS	NA	39
Acaryochloris marina	Cyanobacterial, cord-like	NA	NA	NS	NA	60
Thermosynechococcus elongates	Cyanobacterial APC core	NA	NA	NS, 2D projection	NA	8
Nostoc flagelliforme	Cyanobacterial, hemidiscoidal	NA	NA	NS, cryo-EM, 3D projection	28 Å	96
Synechocystis sp. PCC6803	Cyanobacterial whole cell	NA	NA	Electron tomography	NA	88
Porphyridium cruentum	Red alga, PBS thylakoid	NA	NA	Electron crystal-lography, 2D projection	NA	6
Thermosynechococcus vulcanus	Cyanobacterial, cross-linked	NA	NA	Cryo-EM, 3D projection	Approximately 30 Å	22
Anabaena sp. PCC 7120	Cyanobacterial, hemidiscoidal	NA	EMD-2821	NS, 3D projection	21 Å	16
Halomicronema hongdechloris	Cyanobacterial (AP-B APC-β)$_3$ dimer	3JBB	EMD-6430	NS, 3D projection	26 Å	53
G. pacifica	Red alga, block-shaped	5Y6P	EMD-6769	Cryo-EM, 3D projection	3.5 Å	97
Synechocystis sp. PCC6803	Cyanobacterial whole cell	NA	EMD-4601/ 4602	Electron tomography	23.6 Å	69
Porphyridium purpureum	Red alga, hemiellipsoidal	6KGX	EMD-9976	Cryo-EM, 3D projection	2.8 Å	57

Abbreviations: APC, allophycocyanin; EM, electron microscopy; EMDB; Electron Microscopy Data Bank; NA, not applicable; NS; negative staining; PBS, phycobilisome; PDB, Protein Data Bank.

3.2. Assembly of Rods by Linker Proteins

Two models, the interlocking model and the molecular skeleton model, have been proposed to explain how rod linkers participate in the rod assembly (37, 55, 90). In the interlocking model, the two hexamers interact with two domains of a single linker protein, with one hexamer interacting with one domain and the other hexamer interacting with the other domain; thus, the hexamers are

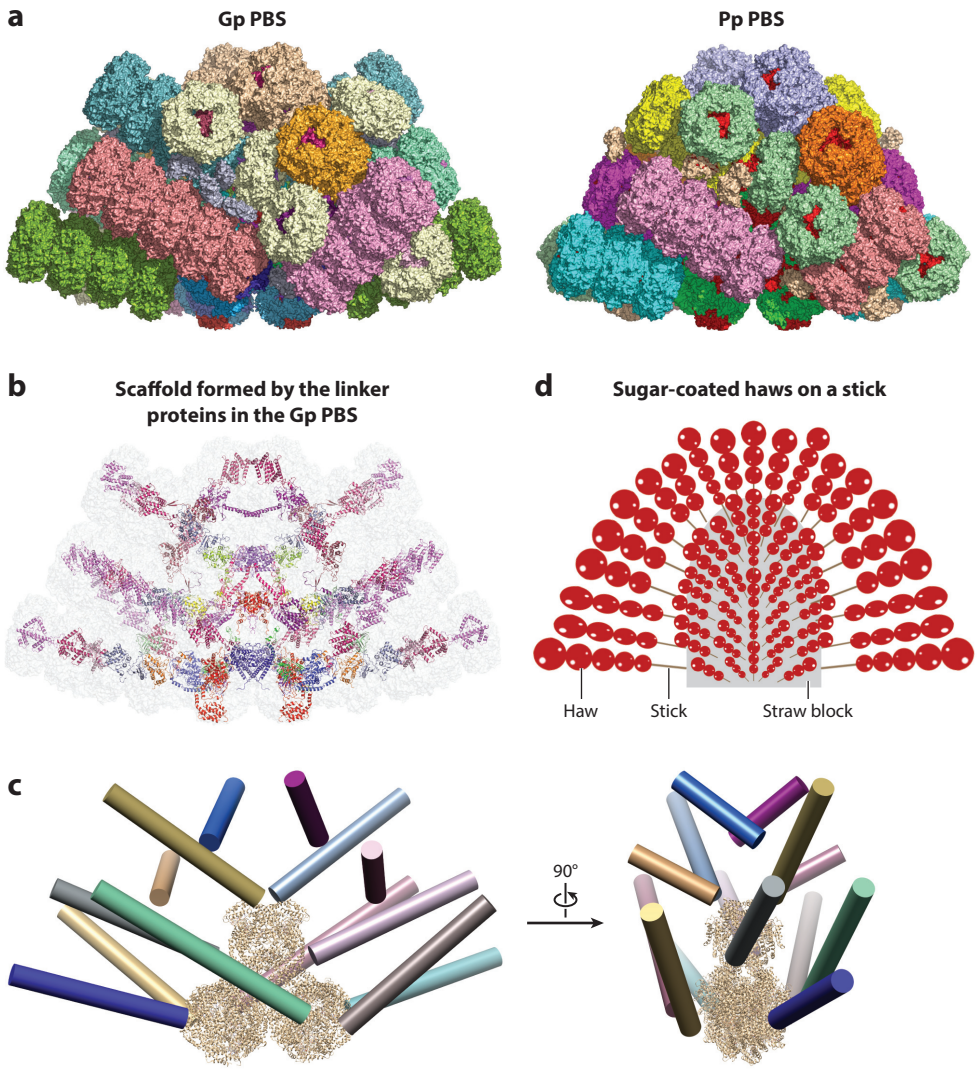

Figure 1

The structure of the phycobilisome (PBS). (*a*) The overall structure of the entire PBS from *Griffithsia pacifica* (GpPBS, *left*) and *Porphyridium purpurium* (PpPBS, *right*), shown in the surface representation. Panel adapted with permission from References 57 and 97. (*b*) The scaffold formed by the linker proteins in the GpPBS from the face view. The linker proteins are shown in the schematic representation, and the phycobiliproteins (PBPs) are shown in the surface representation. Panel adapted with permission from Reference 97. (*c*) The structure of the whole GpPBS in the face view and side view. Each rod is shown as a cylinder, and the core is shown in the schematic representation. (*d*) Sugar-coated haws on a stick.

interlocked by the linker protein. For example, two domains of L_R (Pfam00427 and Pfam01383) contact two adjacent hexamers, leading to the assembly of the rod. The interaction between linker proteins is not emphasized in this model. However, in the molecular skeleton model, the specific interaction between linker proteins acts as the skeleton for the rod assembly.

The structures of the GpPBS and PpPBS indicate that both the interlocking model and the skeleton model are needed to explain the rod architecture of the red algal PBS (**Figure 2*a***). For

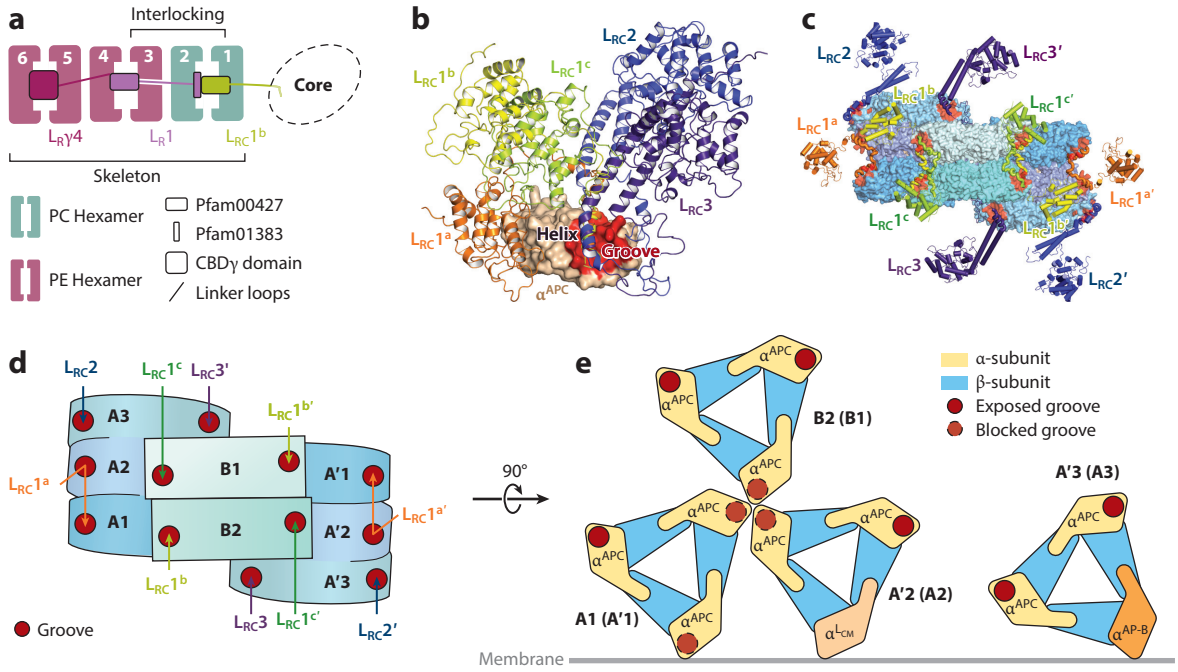

Figure 2

Assembly of the rod and organization of the rod and core by linker proteins. (*a*) Both the interlocking model and the skeleton model exist in the rod architecture of the rod Rb from the phycobilisome (PBS) of *Porphyridium purpurium* (PpPBS). (*b*) Superimposition of the α^{APC} subunits and the spatial positions of their interacting L_{RC} proteins. The alignments were performed using the α^{APC} subunit as a reference. The contacting helices of all L_{RC} proteins are also aligned very well. The groove on the α-subunits that contact the linker helices is shown in red. Panel adapted with permission from Reference 97. (*c*) Interactions between $L_{RC}1$–3/$L_{RC}1'$–3′ and the core. The grooves on the α-subunits that contact the linker helices are shown in red. (*d*) Schematics of the arrangement of L_{RC}s with the core in the red algal PBS. The grooves on the α-subunits that contact the linker helices are indicated with red circles. (*e*) The distribution of the grooves on the middle plane formed by the trimers A1 (A′1), A′2 (A2), and B2 (B1) and the trimer A′3 (A3).

example, the rod Rb from PpPBS contains three hexamers (one PC hexamer and two PE hexamers from the core-proximal end to the core-distal end) and three linker proteins (L_{RC}, L_R, and $L_R\gamma$ from the core-proximal end to the core-distal end). On the one hand, the L_R contains a Pfam01383 domain at its C-terminal region and a Pfam00427 domain at its N-terminal region. These two domains interact with the core-proximal PC hexamer and the neighboring PE hexamer, respectively, which is in agreement with the interlocking model. On the other hand, the three linker proteins interact with each other sequentially, i.e., the L_{RC} contacts the L_R, and the L_R contacts the $L_R\gamma$, which leads to the formation of the rod linker skeleton for the rod assembly. The linker protein $L_R\gamma$ was previously described as the γ-subunit of PE and bears 3–6 chromophores. This type of γ linker protein contains a conserved chromophore binding domain (CBDγ) occupying the central cavity of the PE hexamer, and only small helices or loops stretched out from the hexamer interact with the rigid domain from core-proximal neighboring linkers. For example, the N terminus of $L_R\gamma4$ interacts with the Pfam00427 domain of L_R1 through polar residues and hydrogen bonds. L_R mediates the interlocking model of rod architecture, and all the linker proteins in the rod participate in the formation of the rod linker skeleton by interacting with each other in a specific order (**Figure 2*a***).

3.3. Organization of Rod and Core

The arrangement between rods and core determines the architecture of the PBS. In the PBSs from Gp and Pp, 10 of 14 rods directly bind to the core by specific interactions between L_{RC}s and the core components. These L_{RC}s all use a conserved helix to attach to a groove of the α-subunit of the core APC via extensive hydrophobic interactions and electrostatic interactions (**Figure 2*b,c***). The core contains eight trimers (A1–A3, A′1–A′3, B1, and B2) and 20 α-subunits of APCs, excluding two $\alpha^{L\text{-}CM}$ molecules and two ApcD molecules; thus, there are 20 grooves that can anchor the L_{RC}s (**Figure 2*d,e***). However, some grooves are blocked at the interface of the top and basal cylinders, as well as by the interactions between trimers and the thylakoid membrane, and only 12 grooves are exposed for L_{RC} binding: one groove provided by each of the A1, A′1, A2, and A′2 trimers and two grooves provided by each of the A3, A′3, B1, and B2 trimers (**Figure 2*d,e***). Usually, one L_{RC} anchors to one groove; however, both grooves of A1(A′1) and A2(A′2) are occupied by one L_{RC} (**Figure 2*d***). Therefore, all 12 exposed grooves are saturated by 10 L_{RC}s: $L_{RC}1^{a}$ binds to two grooves from A1 and A2, $L_{RC}1^{a'}$ binds to two grooves from A′1 and A′2, $L_{RC}1^{c}$ and $L_{RC}1^{b'}$ bind to two grooves from B1, $L_{RC}1^{b}$ and $L_{RC}1^{c'}$ bind to two grooves from B2, $L_{RC}2$ and $L_{RC}3'$ bind to two grooves from A3, and $L_{RC}2'$ and $L_{RC}3$ bind to two grooves from A′3. This is consistent with there being 10 rods that directly associate with the core (**Figure 2*c,d***). Sequence alignment studies indicate that the helix residues of the L_{RC} proteins and the groove residues in the α-subunit of the core APC involved in the interactions are highly conserved and contain either hydrophobic or charged and/or polar amino acids throughout the red algae and cyanobacteria, which suggests that the rod–core linker proteins may use a common mechanism when attaching rods to the core during PBS assembly.

3.4. Novel Proteins Functioning as Rod–Core Linkers

In addition to the L_{RC} linkers containing the conserved Pfam00427 domains, another group of proteins that function in the linking of the rods to the core, namely $L_{RC}4$, $L_{RC}5$, and $L_{RC}6$, were found for the first time in the high-resolution structures of PBSs, and their structure is very different from that of the other linkers (97). The common features of these proteins are a structural element in the middle and extensions at both sides. The structural element, containing a long α-helix in $L_{RC}4$ and $L_{RC}5$ and a FAS1 domain in $L_{RC}6$, attaches to the core, and both extensions have extensive contacts with the surrounding proteins from both the core and the rods. Therefore, the revealed structures suggest that $L_{RC}4$–6 function as linkers by anchoring themselves to the core via their middle structural elements and using the extensions as ropes to maintain the stability of the assembled complex.

3.5. Comparison of Structures of Phycobilisomes from the Different Red Algae Species

Two structures of the intact PBSs, the GpPBS and the PpPBS, have been resolved at high resolution. Although the PpPBS has been classified as a hemiellipsoidal PBS, it shares high structural conservation with the block-shaped GpPBS, as described above. The most significant difference between them is their size (**Figure 1*a***). When these two PBSs are superimposed together, the PpPBS is aligned well with the GpPBS but is smaller in size. Indeed, the molecular mass of the PpPBS is 14.7 MDa, whereas that of the GpPBS is 18.0 MDa. Consistent with this, the number of PE hexamers in each of the rods directly binding to the core is one fewer in the PpPBS than in the GpPBS, and the extra PE hexamers are two fewer in the PpPBS than in the GpPBS due to the short lengths of some rods that hold the hexamers. Along with this, the total number of rod

linker proteins of the PpPBS is 12 fewer than that in the GpPBS. In addition to the difference in the number of linker proteins, the types of linker proteins are also different in some cases. In the extra PE hexamer Hd, the linker protein in the PpPBS contains the Pfam00427 domain, whereas that in the GpPBS contains the CBDγ domain.

All of these structural differences lead to there being a lower number of total bilins in the PpPBS (1,598 bilins) than in the GpPBS (2,048 bilins). Another important difference is the presence of a higher number of phycourobilins (PUBs) in the GpPBS; this occurs because all PUBs in the PpPBS come solely from the $L_R\gamma$ proteins, whereas in the GpPBS—besides the $L_R\gamma$ proteins—all PE β-subunits also contain PUBs, giving rise to a higher number of PUBs. The different amount and types of bilins are consistent with the different environments in which the two red algae live. Gp live approximately 20 meters beneath the sea surface, where the major light available is green light (498 nm), which is the maximum absorption wavelength of PUBs, and the light intensity is low. In such a habitat, more PUBs and total bilins can significantly increase the light-harvesting efficiency. Pp live at the sea surface, where the light intensity is higher compared with that under the sea surface; thus, the reduced amount of bilins is sufficient for light capture. All of the structural differences between the PBSs from these two red algae are in accordance with their functions in the effective absorption of light energy in habitats of different light quality and intensity.

4. STRUCTURAL BASIS OF ENERGY TRANSFER IN PHYCOBILISOMES

4.1. Nature of the π–π Interactions

Intermolecular π–π interactions contribute to molecular biology as a constructive noncovalent force, e.g., in the stability of the DNA base pair (12, 63), protein structure and function (14), protein interaction with small molecules (52), and porphyrin aggregation (1). The π–π interactions can be subdivided into three categories on the basis of the geometry of the two aromatic species: parallel configurations, parallel-displaced configurations, and edge-to-face T-shaped configurations (87, 91) (**Figure 3*a***). The parallel-displaced and edge-to-face T-shaped configurations are significantly preferred over parallel geometry in proteins (44, 87). Hunter & Sanders (47) developed an electrostatic model proposing that the geometries of π–π configuration are controlled by electrostatic interactions. In this model, the distribution of the electrostatic potential of an aromatic group consists of a negative electrostatic potential (π-electron cloud) spread above and below the aromatic face and a positive electrostatic potential (along the σ-framework) around the periphery, suggesting that the π–π repulsions and π–σ attractions are the determining factors in π–π interactions (47, 63). In the parallel configuration, where two aromatic rings face each other, the negatively charged electron cloud of two rings coming close to each other is repulsive and is not favored for the stabilization of the two rings (47). However, this configuration can be transformed into a favorable geometry where one aromatic ring is rotated up to 90° (edge-to-face T-shaped configurations) or one aromatic ring is offset laterally within 6 Å (parallel-displaced configurations) (47, 48) (**Figure 3*b***). In addition to the π–π interactions, the cation–π interactions also play an important role, specifically for the stabilization of biomolecules (23, 58) (**Figure 3*a***). Cation–π interactions could occur between the cationic sidechains (arginine and lysine) and the aromatic amino acids (tyrosine, phenylalanine, tryptophan and heteroatom histidine) (31, 72). Cation–π interaction is electrostatic in nature, with the sidechains of positively charged residues forming favorable interactions with the π-electron cloud of the aromatic rings (13, 20). Numerous studies have reported that cation–π interactions are prevalent in protein folding, with the positively charged sidechains preferring to locate above aromatic rings to increase the interactions (10, 30, 64).

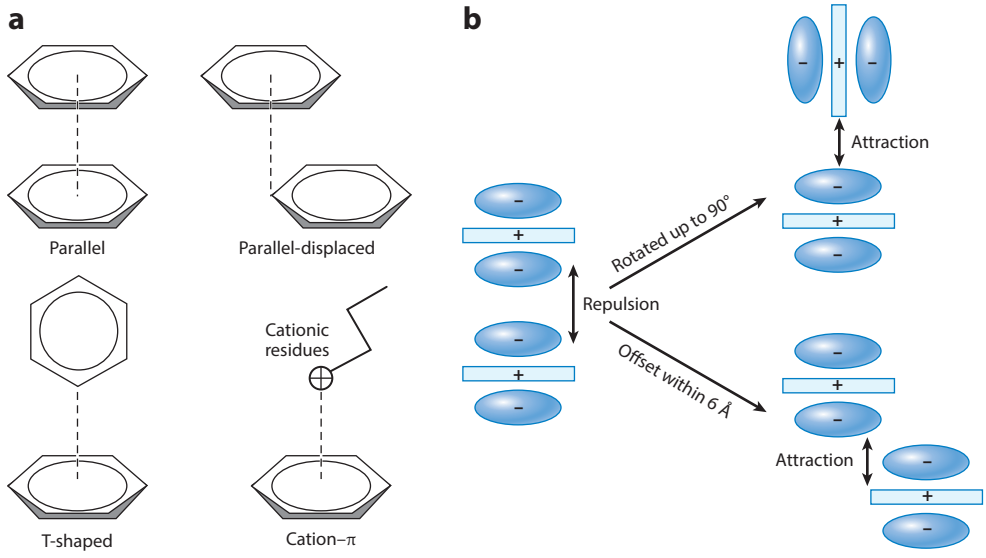

Figure 3

Nature of π–π interactions. (*a*) The types of π–π interactions. The geometries shown are parallel, parallel-displaced, edge-to-face T-shaped, and cation–π configurations. (*b*) Interaction between two idealized π systems as a function of orientation. Two attractive geometries and the repulsive face-to-face geometry are illustrated.

4.2. Energy State and Dihedral Angles of Chromophores

The four open-chain tetrapyrrole chromophores [phycoerythrobilin (PEB), PUB, phycoviolobilin (PVB), and PCB], due to the variation in the conjugation of their double bonds, absorb light at different wavelengths and transfer the energy from high-energy to low-energy chromophores (55, 59, 85) (**Figure 4**). Among these chromophores, PUB has the least conjugation. Rings A and D of PUB are connected with rings B and C by single bonds, and only rings B and C form a conjugated π system, indicating that rings B and C are coplanar, and A and B are out of the B–C plane with varying dihydral angles. PEB and PVB have an extended conjugation on the pyrroles, with three rings forming a conjugated π system and one ring that has a varying dihydral angle. PCBs form a complete conjugated system with all of the rings being coplanar in nature. Thus, dihedral angles between the ring planes of the chromophore are useful in estimating the energy of that chromophore. Duerring et al. (27) and Scharnagl & Schneider (73, 74) have also proposed that the change in the dihedral angles of pyrrole rings determines the energy state of the chromophores. Rings B and C of all of the chromophores mentioned above are almost coplanar, and the increase of the dihedral angles of rings A and D reduces the conjugation of the chromophores, inducing a blue shift in the fluorescence emission spectrum, indicating their higher energy. The crystal structure of R-PE from *Polysiphonia urceolata* was resolved at 1.9 Å resolution (50), and the exact dihedral angle of the PUB was calculated from this high-resolution structure. Recently, a higher-resolution cryo-EM structure of the entire PpPBS was resolved at 2.8 Å (57). The energy state differences among the bilins can be qualitatively estimated by calculating the dihedral angles in their near-native condition. Similar to the crystal structure of R-PE, the dihedral angles Φ_1, Ψ_1, Φ_2...are defined by the plane NA–C(4)–C(5)–C(6), C(4)–C(5)–C(6)–NB, NB–C(9)–C(10)–C(11)..., etc. (**Figure 4*b***); (Φ_1, Ψ_1) is defined as the angle of ring A deviated from ring B (D_{AB}), (Φ_2, Ψ_2) is the angle of ring B deviated from ring C (D_{BC})..., etc. (57). Based on this dihedral angle theory, Ma and coworkers (57) calculated the dihedral angles of the PEB, PUB, and PCB

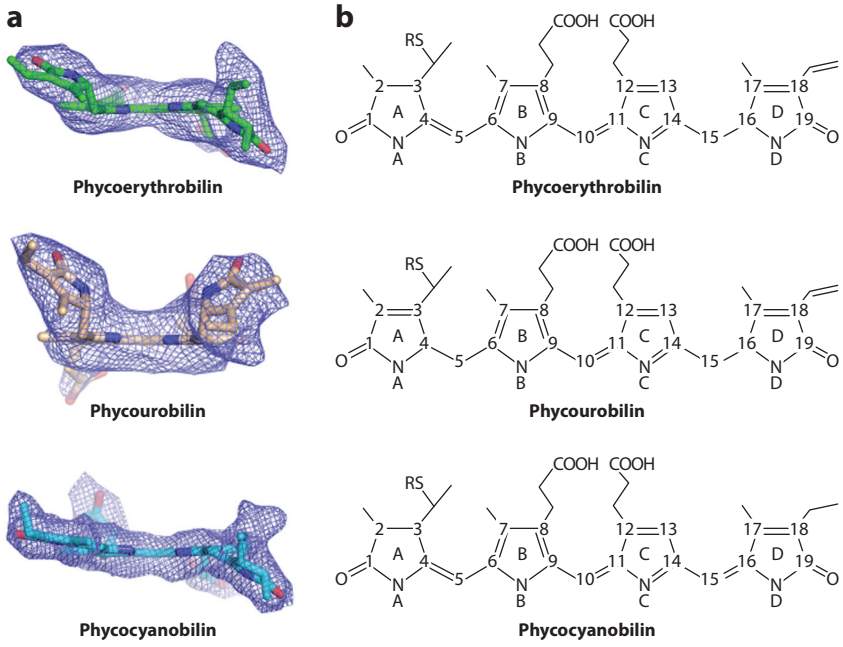

Figure 4

The densities and chemical structures of the types of chromophores. (*a*) Densities of the representative phycoerythrobilin, phycourobilin, and phycocyanobilin bilins show their different coplanarities. (*b*) Chemical structures of three kinds of chromophores. Figure adapted with permission from Reference 57.

of PpPBS. The sum of absolute values of dihedral angles ($|D_{AB}| = |\Phi_1| + |\Psi_1|$, $|D_{BC}| = |\Phi_2| + |\Psi_2| \ldots$) is defined as the deviation of the rings of different bilins. $|D_{AB}|$ of the PUB is 122.5, which is greater than that of the PEB (47.7), PCB (27.9), and PCB/L_{CM} (0.1), indicating that ring A of the PUB deviates from the molecular plane defined by the plane with rings B and C, and the deviation is greater than that of the PEB and PCB. Similarly, $|D_{CD}|$ of both the PEB (130.2) and PUB (128.3) are much higher than that in the PCB (18.2) due to the single bonds present between rings C and D, which allow an unrestricted conformation of ring D with respect to ring C. $|D_{ABCD}|$ ($|D_{ABCD}| = |D_{AB}| + |D_{BC}| + |D_{CD}|$) is used to analyze the conjugation of the entire chromophore. $|D_{ABCD}|$ of the PCB (48.1) and of the terminal emitter L_{CM} PCB (0.7) are much lower than those of the PUB (268.3) and PEB (183), suggesting that the four pyrroles of the PCB are in approximately the same plane and have greater conjugation. Thus, the energy state of the PCB is lower than that of the PEB and PUB according to the calculated dihedral angles.

4.3. Energy Flow in the Rods

The light energy is absorbed by the peripheral rods and transferred to the core and, eventually, to PSI and PSII (7, 56, 86). The PE and PC $(\alpha\beta)_3$ trimers are the basic structural units of the peripheral rods. Several experimental studies have shown that, in each trimer, the absorbed energy is rapidly transferred from the outer bilins to the inner bilins (38, 94). In the PpPBS, each α/β monomer of PE carries five PEB bilins at α82, α139, β61, β82, and β158 (**Figure 5*a***). The conformation of the outmost bilin α139PEB is different from the other four PEBs, as the map density of α139PEB is weaker than the others (**Figure 5*b*,*c***), suggesting that this bilin is more flexible and has less conjugation compared to the others. A key residue, aspartic acid (Asp85), is on the

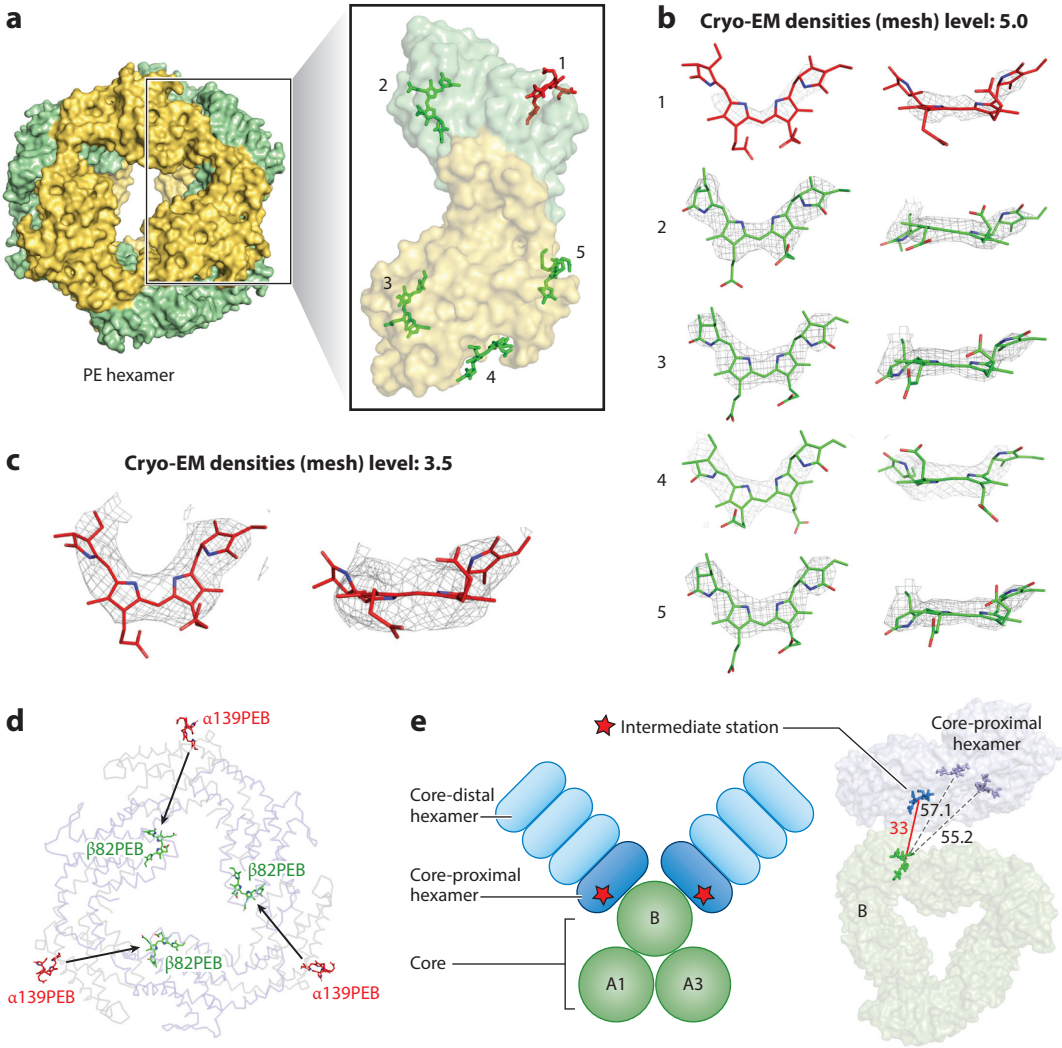

Figure 5

Energy flow in the rod. (*a*) The distribution of chromophores in an α/β monomer of PE: 1, α139PEB; 2, α82PEB; 3, β82PEB; 4, β61PEB; 5, β158PEB. (*b*) The densities of chromophores in an α/β monomer at 5.0 σ. (*c*) The densities of α139PEB (chromophore 1) at 3.5 σ. (*d*) Schematic diagram of the energy transfer pathway in a trimer of rods. (*e*) The intermediate station in rods. Panel adapted with permission from Reference 57. Abbreviation: cryo-EM, cryo-electron microscopy.

side of the PEBs of α82, β61, β82, and β158, forming two H-bonds with the pyrrolic nitrogen of rings B and C, holding these rings in place. However, compared to these PEBs, the α139PEB has less interaction with the surroundings; in particular, the lack of the Asp85 resulted in decreased stabilization of the PEB rings B and C. Thus, in the trimer of the rod, the outmost α139PEB, which has higher energy for the first excited state, will transfer the absorbed energy to the inner stable bilins accordingly (**Figure 5*d***).

For the core-distal hexamers of various rods, three β82 bilins of the inner cavity of $(\alpha\beta)_3$ trimers are arranged in a triangle fashion and interact with the $L_R\gamma$ linker proteins ($L_R\gamma4$ or $L_R\gamma5$). Three aromatic residues (phenylalanine or tyrosine) of the $L_R\gamma$ are located above ring D of the three

β82 bilins, respectively, and induce geometrical changes in the D rings due to the strong π–π interactions. Moreover, an extra PEB from the $L_R\gamma$ has been found to be in close proximity to one of the three β82 bilins (named as the bilin-β_2^{82}), and the distance between them is within 3.0 Å. It is clear that the two specific bilins are strongly coupled, forming the delocalized electronic state with low energy. Compared to the other two β82 bilins, the π-electron clouds of the bilin-β_2^{82} are subjected to greater modulation and may therefore provide an important site of light harvesting and energy migration in the inner cavity of rods. A similar pathway was also observed in a R-PE crystal structure (50).

In the core-proximal hexamer, three β82 bilins are located in the inner cavity of $(\alpha\beta)_3$ trimers. Similar to the core-distal trimers, they also interact with the L_{RC} linker protein ($L_{RC}1$). A histidine (H58) from $L_{RC}1$ is located above the β_2^{82} within 3.0 Å, forming a strong parallel-displaced π–π interaction with its B and C rings. This key histidine residue of $L_{RC}1$ is conserved across different species of red algae and cyanobacteria, indicating its crucial role in fine-tuning and channeling the bilins' energy. Moreover, the β_2^{82} also has the shortest distance (approximately 30 Å) to the core compared to the other two β82 bilins. Thus, it is highly possible that the β_2^{82} of the core-proximal hexamer of rods might act as an intermediate station where the energy converges from the rods and then flows into the core (**Figure 5*e***).

4.4. Key Bilins in the Core

The core contains APCs. In contrast to the R-PC trimers, which have an absorption maximum at 621 nm, APC trimers have a 650-nm absorption maximum, suggesting that the PCBs in the core are at a lower energy state. PCBs in the core are subjected to different π–π interactions with the linker proteins (L_C and L_{CM}), which fine-tunes the energy state of the core bilins. Ma and coworkers (57) analyzed the microenvironments of the key bilins of the core, including two terminal emitter bilins (${}^{A3}\alpha^{81}{}_{ApcD}$ and ${}^{A2}\alpha^{186L_{CM}}$), as illustrated in **Figure 6**. The top cylinder B is far from the basal cylinders in the core, which receive energy from the rods and transfer it to the lower-energy APCs. A phenylalanine of L_{CM}, present at a distance of approximately 5 Å from the β_3^{81} PCB of trimer B (named as B-β_3^{81}), forms a T-shaped π–π interaction. However, the other five key bilins in the two basal cylinders participate in the π–π interactions with linker proteins at shorter distances (within 4 Å). For example, in the bilins A_2-β_1^{81}, A_3-β_2^{81}, and A_1-β_1^{81}, an aromatic residue is located at a distance of approximately 3 Å on rings C and D, forming a significantly preferred parallel-displaced π–π interaction. Moreover, the other two key bilins of trimer A_1' and A_2 (A_1'-β_3^{81} and A_2-β_2^{81}) interact with more than two aromatic residues of L_{CM} at nearly 4 Å, forming more π–π interactions than the other four key bilins (**Figure 6*a*,*b***). These π–π interaction differences seem to modulate these key bilins to a variety of energy states, facilitating energy transfer. Energy in the core is finally transferred to the two PCB chromophores of terminal emitters, ${}^{A3}\alpha^{81}{}_{ApcD}$ and ${}^{A2}\alpha^{186L_{CM}}$. Both ${}^{A3}\alpha^{81}{}_{ApcD}$ and ${}^{A2}\alpha^{186L_{CM}}$ display almost planar conformations, as shown by the high-resolution cryo-EM structure of PpPBS and the crystal structures of ApcD and engineered αL_{CM} [28, 33]. It has been found that several well-conserved aromatic residues are located around the ${}^{A3}\alpha^{81}{}_{ApcD}$, forming different types of π–π interactions, which are necessary to modulate the conjugated π system. In particular, Y65 and W87 have been found to be most important for ${}^{A3}\alpha^{81}{}_{ApcD}$. Y65 only exists in ApcD, which forms a T-shaped π–π interaction with ring A, whereas it is replaced by a valine in other α81 bilins of the core. Tryptophan (W87) forms a 3.6-Å T-shaped π–π interaction with ring D. Both of these residues could effectively expand the delocalization of π electrons of ${}^{A3}\alpha^{81}{}_{ApcD}$ (**Figure 6*c***). Another terminal emitter, ${}^{A2}\alpha^{186L_{CM}}$, also exhibits a lower energy state than upstream PCBs. In addition to the unexpected coplanar geometry (*ZZZssa* conformer), tryptophan (W154) is another crucial factor for modulating the

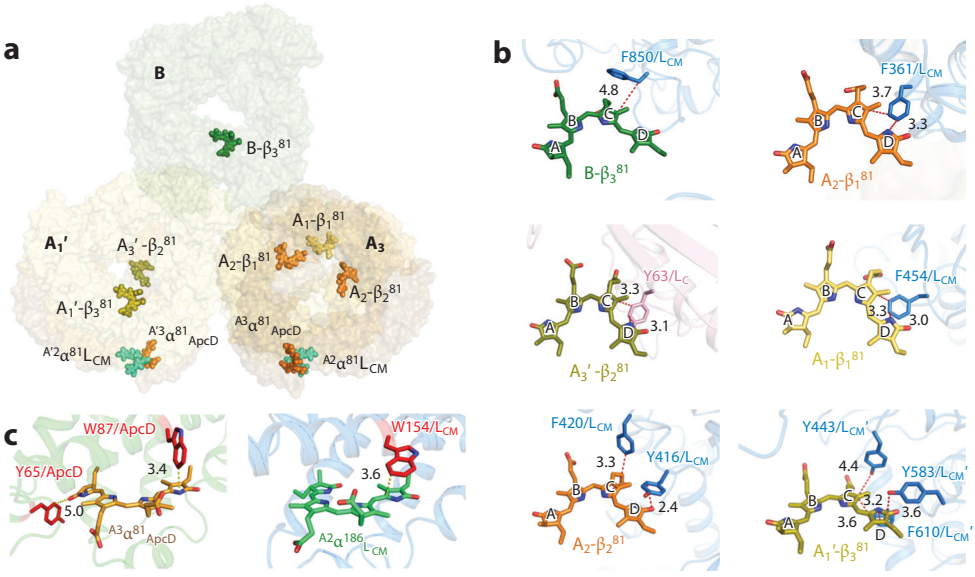

Figure 6

Key bilins in the core. (*a*) Positions of key bilins in the core. (*b*) Interactions between six key bilins and the linker proteins in the core. (*c*) Key π–π interactions of the two terminal emitters, ${}^{A3}\alpha^{81}{}_{ApcD}$ in ApcD (*left*) and ${}^{A2}\alpha^{186}{}_{LCM}$ in L_{CM} (*right*). Figure adapted with permission from Reference 57.

energy state of ${}^{A2}\alpha^{186}L_{CM}$, which is parallel to ring D of the bilin at 3.6 Å (**Figure 6*c***). This unique preference for the sidechain of tryptophan enhances the delocalization of π electrons to ${}^{A2}\alpha^{186}L_{CM}$.

5. OUTLOOK

The high-resolution cryo-EM structures of the complete GpPBS and PpPBS facilitate and improve our understanding of the functions of linker proteins in the energy transfer pathway. The linker proteins not only control the assembly of PBPs into PBSs, but also play an essential role in the energy modulation of the chromophores through various types of π–π interactions. The π–π interaction is a typical noncovalent electric force that is observed in many protein complexes and usually plays an important but secondary role, alongside dominant interactions such as the hydrophobic interaction, hydrogen bond, and salt bridge, in the protein structure and function. In the case of PBSs, π–π interactions play a different but predominant role. In this energy transfer process, the chromophores are the key players, and π electrons of the conjugated four open-chain tetrapyrrole moieties act as the energy carrier. These chromophores form a continuous energy transfer chain and form stable π–π interactions and cation–π interactions with the linker proteins. Even though recent PBS structural studies have revealed many insights into the pathway of light harvesting and energy transfer, we still have a long way to go to understand the complete mechanism and pathway of the entire energy-converting machinery.

Resolving chromophore structures and their individual conformations is fundamental to understanding the PBS energy transfer mechanism. Although the PpPBS has been resolved at a near-atomic resolution of 2.8 Å, many chromophore densities are still opaque and not yet clear, which has limited the analysis of the chromophore conformations at highest precision. To determine the final chromophore model, several parameters, including electron state density, dihedral angle, relative orientation, distance, and spatial distribution, are essential for theoretical

computation. Since the resolution of the EM structures of the chromophores is directly correlated to obtaining their precise conformation and, thus, a better understanding of the PBS energy transfer pathway, continued progress in improving the resolution of the PBS structure is required.

Study of the microenvironment around the chromophores has revealed that some special chromophores are in close contact with some residues from the linker proteins and thus could be acting as the modulators in fine-tuning the energy states of the chromophores. To examine the effect of these interactions on the energy transfer efficiency in vivo, we need to mutate the residues involved in the interactions and measure energy transfer efficiencies of wild-type and mutated PBSs with high-resolution spectroscopic techniques.

The next step in elucidating the energy-converting machinery is to understand how the PBS delivers excitation energy to the reaction centers. Due to our lack of a complete structure of the PBS–PSI/PSII supercomplex, the precise interactions involving PBSs and PSI/PSII have proven to be challenging to elucidate. Weak interactions between PBSs and PSI/PSII have made it difficult to study the PBS–PSI/PSII system using single-particle analysis. With recent advances in the field of cryo-electron tomography, it has become possible to overcome this difficulty and obtain a complete picture of the PBS–PSI/PSII supercomplex, which would be the next step in improving our understanding of the energy conversion pathway.

DISCLOSURE STATEMENT

The author is not aware of any affiliations, memberships, funding, or financial holdings that might be perceived as affecting the objectivity of this review.

ACKNOWLEDGMENTS

The author thanks Jianfei Ma, Xin You, Shan Sun, and C. Sudheer Kumar for their help in the preparation of this review.

LITERATURE CITED

1. Abraham RJ, Eivazi F, Pearson H, Smith KM. 1976. π–π aggregation in metalloporphyrins: causative factors. *J. Chem. Soc. Chem. Commun.* 17:699–701
2. Adir N. 2006. Assembly and disassembly of phycobilisomes. *Microbiol. Monogr.* 2:47–77
3. Adir N, Dobrovetsky Y, Lerner N. 2001. Structure of C-phycocyanin from the thermophilic cyanobacterium *Synechococcus vulcanus* at 2.5 Å: structural implications for thermal stability in phycobilisome assembly. *J. Mol. Biol.* 313:71–81
4. Adir N, Lerner N. 2003. The crystal structure of a novel unmethylated form of C-phycocyanin, a possible connector between cores and rods in phycobilisomes. *J. Biol. Chem.* 278:25926–32
5. Adir N, Vainer R, Lerner N. 2002. Refined structure of C-phycocyanin from the cyanobacterium *Synechococcus vulcanus* at 1.6 Å: insights into the role of solvent molecules in thermal stability and co-factor structure. *Biochim. Biophys. Acta* 1556:168–74
6. Arteni AA, Liu LN, Aartsma TJ, Zhang YZ, Zhou BC, Boekema EJ. 2008. Structure and organization of phycobilisomes on membranes of the red alga *Porphyridium cruentum*. *Photosynth. Res.* 95:169–74
7. Ashby MK, Mullineaux CW. 1999. The role of ApcD and ApcF in energy transfer from phycobilisomes to PSI and PSII in a cyanobacterium. *Photosynth. Res.* 61:169–79
8. Barber J, Morris EP, da Fonseca PCA. 2003. Interaction of the allophycocyanin core complex with photosystem II. *Photochem. Photobiol. Sci.* 5:536–41
9. Brejc K, Ficner R, Huber R, Steinbacher S. 1995. Isolation, crystallization, crystal structure analysis and refinement of allophycocyanin from the cyanobacterium *Spirulina platensis* at 2.3 Å resolution. *J. Mol. Biol.* 249:424–40

10. Brocchieri L, Karlin S. 1994. Geometry of interplanar residue contacts in protein structures. *PNAS* 91:9297–301
11. Bryant DA, Guglielmi G, Tandeau de Marsac N, Castets AM, Cohen-Bazire G. 1979. Structure of cyanobacterial phycobilisomes: model. *Arch. Microbiol.* 123:113–27
12. Burley SK, Petsko GA. 1985. Aromatic-aromatic interaction: a mechanism of protein structure stabilization. *Science* 229:23–28
13. Burley SK, Petsko GA. 1986. Amino-aromatic interactions in proteins. *FEBS Lett*. 203:139–43
14. Burley SK, Petsko GA. 1988. Weakly polar interactions in proteins. *Adv. Protein Chem.* 39:125–89
15. Camara-Artigas A, Bacarizo J, Andujar-Sanchez M, Ortiz-Salmeron E, Mesa-Valle C, et al. 2012. pH-dependent structural conformations of B-phycoerythrin from *Porphyridium cruentum*. *FEBS J*. 279:3680–91
16. Chang L, Liu X, Li Y, Liu CC, Yang F, et al. 2015. Structural organization of an intact phycobilisome and its association with photosystem II. *Cell Res*. 25:726–37
17. Chang WR, Jiang T, Wan ZL, Zhang JP, Yang ZX, Liang DC. 1996. Crystal structure of R-phycoerythrin from *Polysiphonia urceolata* at 2.8 Å resolution. *J. Mol. Biol.* 262:721–31
18. Contreras-Martel C, Martinez-Oyanedel J, Bunster M, Legrand P, Piras C, et al. 2001. Crystallization and 2.2 Å resolution structure of R-phycoerythrin from *Gracilaria chilensis*: a case of perfect hemihedral twinning. *Acta Crystallogr. D Biol. Crystallogr.* 57:52–60
19. Contreras-Martel C, Matamala A, Bruna C, Poo-Caamano G, Almonacid D, et al. 2007. The structure at 2 Å resolution of phycocyanin from *Gracilaria chilensis* and the energy transfer network in a PC-PC complex. *Biophys. Chem.* 125:388–96
20. Crowley PB, Golovin A. 2005. Cation–π interactions in protein–protein interfaces. *Proteins Struct. Funct. Bioinform.* 59:231–39
21. Dagnino-Leone J, Figueroa M, Mella C, Vorphal MA, Kerff F, et al. 2017. Structural models of the different trimers present in the core of phycobilisomes from *Gracilaria chilensis* based on crystal structures and sequences. *PLOS ONE* 12:e0177540
22. David L, Prado M, Arteni AA, Elmlund DA, Blankenship RE, Adir N. 2014. Structural studies show energy transfer within stabilized phycobilisomes independent of the mode of rod–core assembly. *Biochim. Biophys. Acta* 1837:385–95
23. Dougherty DA. 1996. Cation-π interactions in chemistry and biology: a new view of benzene, Phe, Tyr, and Trp. *Science* 271:163–68
24. Doust AB, Marai CN, Harrop SJ, Wilk KE, Curmi PM, Scholes GD. 2004. Developing a structure–function model for the cryptophyte phycoerythrin 545 using ultrahigh resolution crystallography and ultrafast laser spectroscopy. *J. Mol. Biol.* 344:135–53
25. Ducret A, Sidler W, Wehrli E, Frank G, Zuber H. 1996. Isolation, characterization and electron microscopy analysis of a hemidiscoidal phycobilisome type from the cyanobacterium *Anabaena* sp. PCC 7120. *Eur. J. Biochem.* 236:1010–24
26. Duerring M, Huber R, Bode W, Ruembeli R, Zuber H. 1990. Refined three-dimensional structure of phycoerythrocyanin from the cyanobacterium *Mastigocladus laminosus* at 2.7 Å. *J. Mol. Biol.* 211:633–44
27. Duerring M, Schmidt GB, Huber R. 1991. Isolation, crystallization, crystal-structure analysis and refinement of constitutive C-phycocyanin from the chromatically adapting cyanobacterium *Fremyella diplosiphon* at 1.66 Å resolution. *J. Mol. Biol.* 217:577–92
28. Elmorjani K, Thomas JC, Sebban P. 1986. Phycobilisomes of wild type and pigment mutants of the cyanobacterium *Synechocystis* PCC 6803. *Arch. Microbiol.* 146:186–91
29. Ficner R, Lobeck K, Schmidt G, Huber R. 1992. Isolation, crystallization, crystal structure analysis and refinement of B-phycoerythrin from the red alga *Porphyridium sordidum* at 2.2 Å resolution. *J. Mol. Biol.* 228:935–50
30. Flocco MM, Mowbray SL. 1994. Planar stacking interactions of arginine and aromatic side-chains in proteins. *J. Mol. Biol.* 235:709–17
31. Gallivan JP, Dougherty DA. 1999. Cation-π interactions in structural biology. *PNAS* 96:9459–64
32. Gantt E. 1975. Phycobilisomes: light-harvesting pigment complexes. *Bioscience* 25:781–88
33. Gantt E, Conti SF. 1965. The ultrastructure of *Porphyridium cruentum*. *J. Cell Biol.* 26:365–81

34. Gantt E, Conti SF. 1966. Granules associated with the chloroplast lamellae of *Porphyridium cruentum*. *J. Cell Biol.* 29:423–34
35. Gantt E, Lipschultz CA. 1972. Phycobilisomes of *Porphyridium cruentum*: 1. Isolation. *J. Cell Biol.* 54:313–24
36. Gantt E, Lipschultz CA. 1980. Structure and phycobiliprotein composition of phycobilisomes from *Griffithsia pacifica* (Rhodophyceae). *J. Phycol.* 16:394–98
37. Gao X, Zhang N, Wei TD, Su HN, Xie BB, et al. 2011. Crystal structure of the N-terminal domain of linker L-R and the assembly of cyanobacterial phycobilisome rods. *Mol. Microbiol.* 82:698–705
38. Gillbro T, Sharkov AV, Kryukov IV, Khoroshilov EV, Kryukov PG, et al. 1993. Förster energy transfer between neighbouring chromophores in C-phycocyanin trimers. *Biochim. Biophys. Acta* 1140:321–26
39. Glauser M, Bryant DA, Frank G, Wehrli E, Rusconi SS, et al. 1992. Phycobilisome structure in the cyanobacteria *Mastigocladus laminosus* and *Anabaena* sp. PCC7120. *Eur. J. Biochem.* 205:907–15
40. Glazer AN. 1985. Light harvesting by phycobilisomes. *Annu. Rev. Biophys. Biophys. Chem.* 14:47–77
41. Grossman AR. 1990. Chromatic adaptation and the events involved in phycobilisome biosynthesis. *Plant Cell Environ.* 13:651–66
42. Guan X, Qin S, Zhao F, Zhang X, Tang X. 2007. Phycobilisomes linker family in cyanobacterial genomes: divergence and evolution. *Int. J. Biol. Sci.* 3:434–45
43. Guglielmi G, Cohenbazire G, Bryant DA. 1981. The structure of *Gloeobacter violaceus* and its phycobilisomes. *Arch. Microbiol.* 129:181–89
44. Hohenstein EG, Sherrill CD. 2009. Effects of heteroatoms on aromatic $\pi-\pi$ interactions: benzene–pyridine and pyridine dimer. *J. Phys. Chem. A* 113:878–86
45. Hu Q, Marquardt J, Iwasaki I, Miyashita H, Kurano N, et al. 1999. Molecular structure, localization and function of biliproteins in the chlorophyll *a/d* containing oxygenic photosynthetic prokaryote *Acaryochloris marina*. *Biochim. Biophys. Acta* 1412:250–61
46. Huber R. 1989. Nobel lecture: a structural basis of light energy and electron transfer in biology. *EMBO J.* 8:2125–47
47. Hunter CA, Sanders JKM. 1990. The nature of π-π interactions. *J. Am. Chem. Soc.* 112:5525–34
48. Hunter CA, Singh J, Thornton JM. 1991. π-π interactions: the geometry and energetics of phenylalanine-phenylalanine interactions in proteins. *J. Mol. Biol.* 218:837–46
49. Jiang T, Zhang JP, Chang WR, Liang DC. 2001. Crystal structure of R-phycocyanin and possible energy transfer pathways in the phycobilisome. *Biophys. J.* 81:1171–79
50. Jiang T, Zhang JP, Liang DC. 1999. Structure and function of chromophores in R-phycoerythrin at 1.9 angstrom resolution. *Proteins Struct. Funct. Genet.* 34:224–31
51. Kumar V, Sonani RR, Sharma M, Gupta GD, Madamwar D. 2016. Crystal structure analysis of C-phycoerythrin from marine cyanobacterium *Phormidium* sp. A09DM. *Photosynth. Res.* 129:17–28
52. Lehn J-M. 1990. Perspectives in supramolecular chemistry—from molecular recognition towards molecular information processing and self-organization. *Angew. Chem. Int. Ed. Engl.* 29:1304–19
53. Li Y, Lin Y, Garvey CJ, Birch D, Corkery RW, et al. 2016. Characterization of red-shifted phycobilisomes isolated from the chlorophyll *f*-containing cyanobacterium *Halomicronema hongdechloris*. *Biochim. Biophys. Acta* 1857:107–14
54. Liu JY, Jiang T, Zhang JP, Liang DC. 1999. Crystal structure of allophycocyanin from red algae *Porphyra yezoensis* at 2.2-Å resolution. *J. Biol. Chem.* 274:16945–52
55. Liu LN, Chen XL, Zhang YZ, Zhou BC. 2005. Characterization, structure and function of linker polypeptides in phycobilisomes of cyanobacteria and red algae: an overview. *Biochim. Biophys. Acta* 1708:133–42
56. Lundell DJ, Glazer AN. 1983. Molecular architecture of a light-harvesting antenna: structure of the 18 S core-rod subassembly of the *Synechococcus* 6301 phycobilisome. *J. Biol. Chem.* 258:894–901
57. Ma J, You X, Sun S, Wang X, Qin S, Sui S-F. 2020. Structural basis of energy transfer in *Porphyridium purpureum* phycobilisome. *Nature* 579:146–51
58. Ma JC, Dougherty DA. 1997. The cation$-\pi$ interaction. *Chem. Rev.* 97:1303–24
59. MacColl R. 1998. Cyanobacterial phycobilisomes. *J. Struct. Biol.* 124:311–34
60. Marquardt J, Senger H, Miyashita H, Miyachi S, Morschel E. 1997. Isolation and characterization of biliprotein aggregates from *Acaryochloris marina*, a *Prochloron*-like prokaryote containing mainly chlorophyll *d*. *FEBS Lett.* 410:428–32

61. Marx A, Adir N. 2013. Allophycocyanin and phycocyanin crystal structures reveal facets of phycobilisome assembly. *Biochim. Biophys. Acta* 1827:311–18
62. McGregor A, Klartag M, David L, Adir N. 2008. Allophycocyanin trimer stability and functionality are primarily due to polar enhanced hydrophobicity of the phycocyanobilin binding pocket. *J. Mol. Biol.* 384:406–21
63. Meyer EA, Castellano RK, Diederich F. 2003. Interactions with aromatic rings in chemical and biological recognition. *Angew. Chem. Int. Ed. Engl.* 42:1210–50
64. Mitchell JBO, Nandi CL, McDonald IK, Thornton JM, Price SL. 1994. Amino/aromatic interactions in proteins: Is the evidence stacked against hydrogen bonding? *J. Mol. Biol.* 239:315–31
65. Murray JW, Maghlaoui K, Barber J. 2007. The structure of allophycocyanin from *Thermosynechococcus elongatus* at 3.5 Å resolution. *Acta Crystallogr. F* 63:998–1002
66. Nield J, Rizkallah PJ, Barber J, Chayen NE. 2003. The 1.45 Å three-dimensional structure of C-phycocyanin from the thermophilic cyanobacterium *Synechococcus elongates*. *J. Struct. Biol.* 141:149–55
67. Padyana AK, Bhat VB, Madyastha KM, Rajashankar KR, Ramakumar S. 2001. Crystal structure of a light-harvesting protein C-phycocyanin from *Spirulina platensis*. *Biochem. Biophys. Res. Commun.* 282:893–98
68. Peng PP, Dong LL, Sun YF, Zeng XL, Ding WL, et al. 2014. The structure of allophycocyanin B from *Synechocystis* PCC 6803 reveals the structural basis for the extreme redshift of the terminal emitter in phycobilisomes. *Acta Crystallogr. D* 70:2558–69
69. Rast A, Schaffer M, Albert S, Wan W, Pfeffer S, et al. 2019. Biogenic regions of cyanobacterial thylakoids form contact sites with the plasma membrane. *Nat. Plants* 5:436–46
70. Reuter W, Wiegand G, Huber R, Than ME. 1999. Structural analysis at 2.2 Å of orthorhombic crystals presents the asymmetry of the allophycocyanin-linker complex, $AP{\cdot}L_C^{7.8}$, from phycobilisomes of *Mastigocladus laminosus*. *PNAS* 96:1363–68
71. Ritter S, Hiller RG, Wrench PM, Welte W, Diederichs K. 1999. Crystal structure of a phycourobilin-containing phycoerythrin at 1.90-angstrom resolution. *J. Struct. Biol.* 126:86–97
72. Rooman M, Liévin J, Buisine E, Wintjens R. 2002. Cation–π/H-bond stair motifs at protein–DNA interfaces. *J. Mol. Biol.* 319:67–76
73. Scharnagl C, Schneider S. 1989. UV-visible absorption and circular dichroism spectra of the subunits of C-phycocyanin I: quantitative assessment of the effect of chromophore–protein interaction in the α-subunit. *J. Photochem. Photobiol. B* 3:603–14
74. Scharnagl C, Schneider S. 1991. UV-visible absorption and circular dichroism spectra of the subunits of C-phycocyanin II: a quantitative discussion of the chromophore–protein and chromophore–chromophore interactions in the β subunit. *J. Photochem. Photobiol. B* 8:129–57
75. Schirmer T, Bode W, Huber R. 1987. Refined three-dimensional structures of two cyanobacterial C-phycocyanins at 2.1 and 2.5 Å resolution: a common principle of phycobilin-protein interaction. *J. Mol. Biol.* 196:677–95
76. Schirmer T, Bode W, Huber R, Sidler W, Zuber H. 1985. X-ray crystallographic structure of the light-harvesting biliprotein C-phycocyanin from thermophilic cyanobacterium *Mastigocladus laminosus* and its resemblance to globin structures. *J. Mol. Biol.* 184:257–77
77. Schirmer T, Huber R, Schneider M, Bode W, Miller M, Hackert ML. 1986. Crystal structure analysis and refinement at 2.5 Å of hexameric C-phycocyanin from the cyanobacterium *Agmenellum quadruplicatum*: the molecular model and its implication for light-harvesting. *J. Mol. Biol.* 188:651–76
78. Schmidt M, Krasselt A, Reuter W. 2006. Local protein flexibility as a prerequisite for reversible chromophore isomerization in alpha-phycoerythrocyanin. *Biochim. Biophys. Acta* 1764:55–62
79. Searle GFW, Barber J, Porter G, Tredwell CJ. 1978. Picosecond time-resolved energy transfer in *Porphyridium cruentum*. 2. In the isolated light harvesting complex (phycobilisomes). *Biochim. Biophys. Acta* 501:246–56
80. Sonani RR, Gupta GD, Madamwar D, Kumar V. 2015. Crystal structure of allophycocyanin from marine cyanobacterium *Phormidium* sp. A09DM. *PLOS ONE* 10:e0124580
81. Sonani RR, Roszak AW, Liu H, Gross ML, Blankenship RE, et al. 2020. Revisiting high-resolution crystal structure of *Phormidium rubidium* phycocyanin. *Photosynth. Res.* 144:349–60

82. Sonani RR, Roszak AW, Ortmann de Percin Northumberland C, Madamwar D, Cogdell RJ. 2018. An improved crystal structure of C-phycoerythrin from the marine cyanobacterium *Phormidium* sp. A09DM. *Photosynth. Res.* 135:65–78
83. Soni BR, Hasan MI, Parmar A, Ethayathulla AS, Kumar RP, et al. 2010. Structure of the novel 14kDa fragment of alpha-subunit of phycoerythrin from the starving cyanobacterium *Phormidium tenue*. *J. Struct. Biol.* 171:247–55
84. Stec B, Troxler RF, Teeter MM. 1999. Crystal structure of C-phycocyanin from *Cyanidium caldarium* provides a new perspective on phycobilisome assembly. *Biophys. J.* 76:2912–21
85. Su HN, Xie BB, Zhang XY, Zhou BC, Zhang YZ. 2010. The supramolecular architecture, function, and regulation of thylakoid membranes in red algae: an overview. *Photosynth. Res.* 106:73–87
86. Tang K, Ding WL, Hoppner A, Zhao C, Zhang L, et al. 2015. The terminal phycobilisome emitter, LCM: a light-harvesting pigment with a phytochrome chromophore. *PNAS* 112:15880–85
87. Thakuria R, Nath NK, Saha BK. 2019. The nature and applications of π–π interactions: a perspective. *Crystal Growth Des.* 19:523–28
88. van de Meene AML, Hohmann-Marriott MF, Vermaas WFJ, Roberson RW. 2006. The three-dimensional structure of the cyanobacterium *Synechocystis* sp. PCC 6803. *Arch. Microbiol.* 184:259–70
89. Wang XQ, Li LN, Chang WR, Zhang JP, Gui LL, et al. 2001. Structure of C-phycocyanin from *Spirulina platensis* at 2.2 Å resolution: a novel monoclinic crystal form for phycobiliproteins in phycobilisomes. *Acta Crystallogr. D* 57:784–92
90. Watanabe M, Ikeuchi M. 2013. Phycobilisome: architecture of a light-harvesting supercomplex. *Photosynth. Res.* 116:265–76
91. Wheeler SE. 2011. Local nature of substituent effects in stacking interactions. *J. Am. Chem. Soc.* 133:10262–74
92. Wilk KE, Harrop SJ, Jankova L, Edler D, Keenan G, et al. 1999. Evolution of a light-harvesting protein by addition of new subunits and rearrangement of conserved elements: crystal structure of a cryptophyte phycoerythrin at 1.63-Å resolution. *PNAS* 96:8901–6
93. Williams RC, Gingrich JC, Glazer AN. 1980. Cyanobacterial phycobilisomes: particles from *Synechocystis* 6701 and 2 pigment mutants. *J. Cell Biol.* 85:558–66
94. Xie S, Du M, Mets L, Fleming G. 1992. Femtosecond fluorescence depolarization study of photosynthetic antenna proteins: observation of ultrafast energy transfer in trimeric C-phycocyanin and allophycocyanin. In *Proc. SPIE 1640: Time-Resolved Laser Spectroscopy in Biochemistry III*, ed. JR Lakowicz, Art. 58278. Bellingham, WA: SPIE
95. Yamanaka G, Glazer AN, Williams RC. 1980. Molecular architecture of a light-harvesting antenna: comparison of wild-type and mutant *Synechococcus* 6301 phycobilisomes. *J. Biol. Chem.* 255:1004–10
96. Yi ZW, Huang H, Kuang TY, Sui SF. 2005. Three-dimensional architecture of phycobilisomes from *Nostoc flagelliforme* revealed by single particle electron microscopy. *FEBS Lett.* 579:3569–73
97. Zhang J, Ma J, Liu D, Qin S, Sun S, et al. 2017. Structure of phycobilisome from the red alga *Griffithsia pacifica*. *Nature* 551:57–63

Annual Review of Biophysics
Volume 50, 2021

Contents

Indexes

Errata

An online log of corrections to *Annual Review of Biophysics articles* may be found at http://www.annualreviews.org/errata/biophys